HHS Public Access

Author manuscript

Acta Biomater. Author manuscript; available in PMC 2017 February 01.

Published in final edited form as:

Acta Biomater. 2016 February ; 31: 156–166. doi:10.1016/j.actbio.2015.11.051.

Human Mesenchymal Stem Cells Cultured on Silk Hydrogels with Variable Stiffness and Growth Factor Differentiate into Mature Smooth Muscle Cell Phenotype

Michael Floren[1,2], **Walter Bonani**[2], **Anirudh Dharmarajan**[1], **Antonella Motta**[2], **Claudio Migliaresi**[2], and **Wei Tan**[1]

[1]Department of Mechanical Engineering, University of Colorado Boulder, Boulder, Colorado 80309

[2]Department of Industrial Engineering and Biotech Research Center, University of Trento, via Sommarive 9, 38123 Trento, Italy

Abstract

Cell-matrix and cell-biomolecule interactions play critical roles in a diversity of biological events including cell adhesion, growth, differentiation, and apoptosis. Evidence suggests that a concise crosstalk of these environmental factors may be required to direct stem cell differentiation toward matured cell type and function. However, the culmination of these complex interactions to direct stem cells into highly specific phenotypes *in vitro* is still widely unknown, particularly in the context of implantable biomaterials. In this study, we utilized tunable hydrogels based on a simple high pressure CO_2 method and silk fibroin (SF) the structural protein of *Bombyx mori* silk fibers. Modification of SF protein starting water solution concentration results in hydrogels of variable stiffness whilst retaining key structural parameters such as matrix pore size and β-sheet crystallinity. To further resolve the complex crosstalk of chemical signals with matrix properties, we chose to investigate the role of 3D hydrogel and transforming growth factor (TGF-β1), with the aim of correlating the effects on the vascular commitment of human mesenchymal stem cells. Our data revealed the potential to upregulate matured vascular smooth muscle cell phenotype (myosin heavy chain expression) of hMSCs by employing appropriate matrix stiffness and growth factor (within 72 h). Overall, our observations suggest that chemical and physical stimuli within the cellular microenvironment are tightly coupled systems involved in the fate decisions of hMSCs. The production of tunable scaffold materials that are biocompatible and further specialized to mimic tissue-specific niche environments will be of considerable value to future tissue engineering platforms.

Graphical abstract

CORRESPONDING AUTHOR: Wei Tan, wtan@colorado.edu, Phone: (303) 492-0239, Fax: 303-492-3498, Address: Departments of Mechanical Engineering, 427 UCB University of Colorado at Boulder, CO 80309-0427, USA.

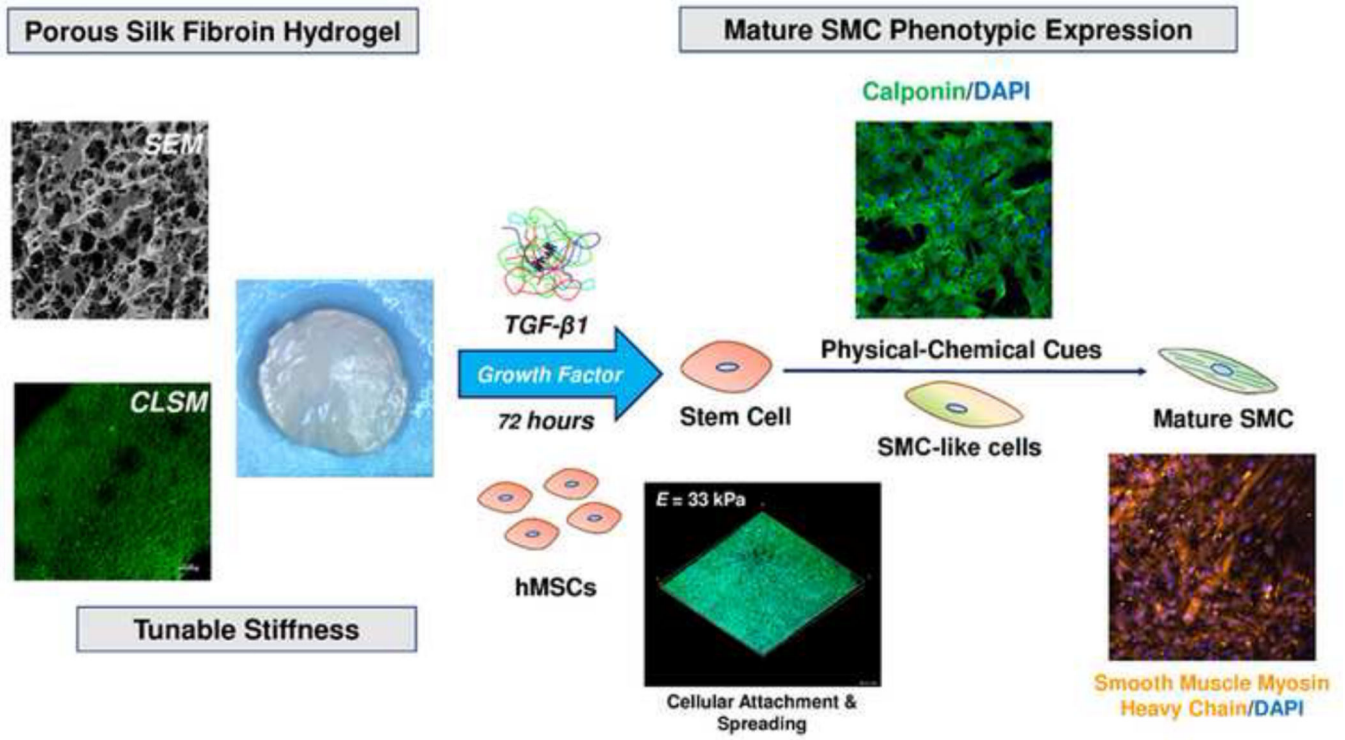

Keywords

silk fibroin; tunable hydrogel; stem cell differentiation; growth factor

1. Introduction

Loss of vascular function associated with cardiovascular disease, such as atherosclerosis, represents the leading medical epidemic in the United States and typically requires surgical intervention through synthetic or autologous vascular grafts [1]. To overcome the limitations associated with adult cell sources, which are often restricted by source or compromised by disease, mesenchymal stem cells (MSCs) have emerged as potential candidates for vascular tissue engineering [2]. However, despite their growing application, several MSC-based vascular regeneration strategies have been met with inconsistent results, and in some cases resulted in abridged vascular function. For instance, direct bolus delivery of MSCs to injured vasculature can lead to a dysfunctional endothelium, resulting in a higher incidence of vessel occlusion compromising vessel mechanics [3]. Likewise, MSCs injected at the site of infarcted hearts resulted in increased levels of calcification and ossification of the surrounding cardiac tissue [4]. These findings suggest a lack of fundamental understanding of the complex vascular niche environment and mechanisms accredited to MSC differentiation towards mature, functional vascular tissues.

Cell interactions with the local microenvironment are recognized in several important biological events including cell adhesion, growth, differentiation, and apoptosis [5, 6]. In particular, substrate biophysical properties such as rigidity [7, 8], geometry [9, 10]

biological ligand [11, 12], soluble factor [13], or combination thereof [14] have been revealed to influence MSC differentiation events. Evidence suggests that a concise crosstalk of these environmental factors may be required to direct MSC differentiation toward desired cell type and function. These findings are supported by recent reports which reveal MSCs acquiring tissue-specific characteristics when co-cultured with mature cells types or exposed to preformed biological matrices *in vitro*, highlighting the important regulatory role elicited by the specific signals of the microenvironment towards stem cell differentiation [15]. However, current methods to regulate stem cell differentiation are often executed independently of other factors, i.e. stiffness or growth factor individually, or lack the amenity to integrate these parameters into a tailorable milieu. A biomimetic approach, incorporating several environmental signals, such as cell-matrix and cell-biomolecule interactions, will help to establish more robust and specific MSC differentiation protocols.

Integration of complex cellular signaling environments into biomaterial scaffolds presents a considerable challenge to the tissue engineering community [16]. A variety of synthetically-formulated as well as natural materials have been evaluated for 3D biomaterial scaffolds [17]. Synthetic materials are attractive for their cost, reproducible fabrication and facile manufacturing yet their lack of cell-recognition sites as well as potential for toxic degradation products causing undesirable inflammation are often disadvantageous [18]. On the contrary, natural materials represent an attractive scaffold platform as they have excellent biological properties, such as cellular recognition, biocompatibility and the potential to degrade through known metabolic processes [19, 20]

Silk fibroin (SF), a natural protein extracted from *Bombyx mori* silkworms, is an attractive material for tissue engineering due to its excellent mechanical properties, biocompatibility, tunable degradation rate, and mild inflammatory response *in vivo* [21]. A diversity of regenerative tissues has been reported using SF-based constructs including bone [22, 23], cartilage [24], vascular [25–27], skin [28], nervous [29], hepatic [30] and ocular [31] amongst others [21]. We previously developed a technique to produce porous, SF hydrogels with tunable stiffness and morphology using the green solvent, carbon dioxide (CO_2) [32]. Hydrogel elastic moduli approaching soft tissues (E = 6–30 kPa), combined with ease of fabrication and biocompatibility, motivated us to use these SF materials as a platform to instruct stem cell differentiation towards the vascular smooth muscle cell (SMC) lineage in a precise manner. In addition to substrate rigidity, chemical signals are important for vascular development, maintenance, and regeneration and collectively constitute a complex process involving the interactions of many cellular features *in vivo* [33]. However, the effects of stiffness and its interaction with growth factors have yet to be sufficiently studied, the resolution of which may provide new insights into processes of cellular regeneration and tissue maintenance as they pertain to the cellular microenvironment.

In the present study, we address cellular differentiation on tunable SF hydrogels prepared from a solvent-free CO_2 processing method. The transforming growth factor β (TGF-β) family is a potent regulator of several cell functions such as proliferation, spreading [34] and is strongly associated with vascular smooth muscle cell (vSMC) differentiation of stem cells [13]. Therefore, the focus of this work is on exploiting the combined use of substrate stiffness and growth factor (TGF-β1) on SF matrices, with the aim of correlating the effects

on the vascular commitment of human mesenchymal stem cells (hMSCs). The production of tunable scaffold materials that are biocompatible and further specialized to mimic vascular niche environments will be of considerable value to future tissue engineering platforms.

2. Materials and Methods

2.1 SF Hydrogel Preparation

Aqueous silk fibroin (SF) solutions were prepared from degummed cocoons of *Bombyx Mori* and subsequently dissolving the obtained fibers in 9.3 M LiBr (Fluka Chemicals, Buchs, Switzerland) aqueous solution (10% w/v) at 65 °C for 4 hours and filtered to eliminate impurities. The obtained SF solution was then placed in Slide-A-Lyzer cassette 3500 Da MWCO (Pierce, Thermo Scientific) and dialyzed against distilled water for 3 days at room temperature to remove residual salts. Following dialysis SF solution volume was adjusted with distilled water to reach the desired concentration. Silk hydrogels were prepared from a previously published protocol using high pressure CO_2 [32]. Briefly, SF solutions at different concentrations (1.5, 2, 3 & 4 wt%) were syringed into a custom Teflon mold consisting of 12 cylindrical specimens (h: 3 mm, Ø 10 mm) and placed within a stainless steel high pressure reaction vessel (BR-300, Berghof Products + Instruments, Eningen, Germany). The temperature of the reactor was controlled through an electrical heating jacket run by a BDL-3000 temperature controller (Berghof). Once the system had been sealed and thermal equilibrium established (40°C), CO_2 gas was introduced in the reactor and pressurized at a working pressure of 60 bar through a high-performance liquid chromatography (HPLC) pump (Model 426, Alltech, Deerfield, IL, USA) and isolated for specific gelation times (0–8 hours). Following the set gelation period, the system was depressurized slowly (approximately 30 minutes) to avoid sample rupture due to the high pressure release. Collected hydrogel specimens were immediately placed in PBS and stored at 4°C for future characterization.

2.2. Hydrogel Structural Characterization

2.2.1. Thermal analysis by differential scanning calorimetry—Following SF hydrogel formation, specimens were shock frozen in liquid nitrogen and subsequently lyophilized to prepare dry samples for thermal analysis. Silk hydrogel thermal properties were acquired using a differential scanning calorimeter (DSC) (Mettler, Model DSC30, Columbus, OH, USA) with N_2 gas flow, at a heating rate of 10 °C/min from 0°C to 350°C.

2.2.2. Fourier-Transform Infrared Spectroscopy (FTIR) analysis—Silk protein structural characteristics were investigated before and after high pressure CO_2 treatment using FTIR Spectrum One (Perking Elmer, Waltham, MA, USA) with a zinc selenide crystal. To preserve the secondary structure of the obtained silk hydrogels, specimens were immediately quenched in liquid nitrogen after treatment by high pressure CO_2 and subsequently lyophilized for 48 hours to obtain dry samples for characterization. Structural data was acquired by loading lyophilized silk hydrogel specimens onto the IR apparatus and sample spectrums were collected as a mean of 32 acquisitions (between 4000 cm^{-1} and 400 cm^{-1}) with a spectral resolution of 4 cm^{-1}. Fourier Self-Deconvolution (FSD) of the infrared spectra spanning the amide I region (1595–1705 cm^{-1}) was employed to quantify the

different silk secondary structures within the hydrogel specimens. Deconvolution was performed using parameters described elsewhere [35]. Following deconvolution, Gaussian curve fitting was then performed with Origin 8.0 (OriginLab Corp., Northampton, MA).

2.2.3. Morphology Assessment—Imaging of dry hydrogel specimens was obtained using a scanning electron microscope (SEM) (Quanta 200 Scanning Electron Microscope – FE – operating mode: low vacuum, gaseous secondary electron GSE detector). Hydrated silk hydrogels were first quenched in liquid nitrogen and subsequently lyophilized for 48 hours to prepare dry cross sections for imaging. Prior to imaging, lyophilized cross sections were sputter coated (Biorad SC500, Hemel Hempstead, UK) with a thin layer of gold to avoid charging of the sample.

Imaging of wet hydrogel specimens was performed by submerging neat SF hydrogel matrices in 0.1 mg/ml Rhodamine123 solution (Sigma) at 4 °C for 8 hours (Rh123 is a greenfluorescent small molecule excitation 485nm, emission 535 nm) and then repeatedly washed in DI water to remove all un-bound dye. The non-specific adsorption of Rh123 within the SF matrices allows for visual observation of the wet hydrogel morphology [36]. Gels were then placed on glass slides for confocal imaging. Samples were imaged with Argon-ion laser at 488nm coupled with a band-pass emission filter 535/15 nm using a confocal microscope Nikon A1 model.

2.2.4. Mechanical Properties in Compression—Silk hydrogel mechanical properties were tested under compression. Compression tests of hydrogel specimens (8 mm diameter × 5 mm depth) were performed in the unconfined state by a Mechanical Testing System (MTS; Eden Prairie, MN) using a 5N load cell. The mechanical properties of the gel samples were tested in the wet state, in PBS, at room temperature. Strain (mm) and load (N) were recorded using Wintest software at a cross speed of 20 μm/s up to 60% strain level. To ensure proper sample placement and flatness, samples were cyclically preconditioned at 1% strain for 10 cycles. The compressive modulus was calculated from the tangent slope of the linear elastic region of the rendered stress/strain curve.

2.3. Cell Culture methods

Human mesenchymal stem cells (hMSCs) were purchased from Lonza (Switzerland) and maintained with Lonza's MSCGM human Mesenchymal Stem Cell Growth BulletKit. Reduced-serum medium consisted of Dulbecco's Modified Eagles Media (DMEM) (Hyclone, Logan/UT), with 1% defined FBS (Hyclone, Logan/UT) and 1% Penn/Strep (Invitrogen, Carlsbad, CA). Cells were cultured and maintained at 37°C and 5% CO_2 with medium being replaced every 72 h. Passages 3–6 were used for all experiments. Silk gels were briefly incubated in reduced-serum medium in 24-well plates and medium was aspirated just prior to seeding. hMSCs were seeded at 5×10^4 cells to the surface of each silk gel using a concentrated cell suspension. Cells were incubated for 1.5 h at 37°C and 5% CO_2 to allow for initial attachment before reduced-serum medium was added to the wells. Recombinant human Transforming Growth Factor-β1 (TGF-β1) was supplied by Novoprotein (Summit, NJ) and was maintained at 10ng/ml for experimental conditions requiring growth factor administration.

2.4. Cell Characterization Methods

2.4.1. Quantitative real-time polymerase chain reaction (qPCR)—Total RNA was extracted from samples using Trizol-chloroform method [37] followed by further purification with RNeasy Kit Microkit (Qiagen) per the manufacturer's instructions. Quantification of RNA was performed on a Nanodrop 2000 spectrophotometer (Thermo Scientific). Single-stranded complementary DNA (ss-cDNA) was synthesized from RNA with iScript cDNA synthesis kit (Bio-Rad) using a Hybaid PCR Express thermal cycler per the manufacturer's instructions. SYBR RT^2-qPCR primer assays from Qiagen were used with iTaq Universal SYBR Green Supermix (Bio-Rad) in this study. The primers used and their corresponding National Center for Biotechnology (NCBI) Reference Sequence (RefSeq) numbers are listed in Table 1. β-actin was the reference gene. Quantitative real-time polymerase chain reaction (qPCR) was performed on either a Bio-rad CFX96 or iQ5 under the following reaction conditions: 95°C for 3 min and 40 cycles of 95°C for 5 s and 60°C for 30 s. Relative expression was calculated using quantification cycle (Cq) values as per the ΔΔCq-method and fold change was calculated using $2^{-\Delta\Delta Cq}$ [38].

2.4.2. Immunofluorescent Staining—Following cell culture, SF hydrogel samples were fixed with 3.7% formaldehyde at room temperature, permeated with 0.1% Triton X-100 and blocked with 3% BSA (Sigma) Immunofluorescent staining of cells for cell nuclei (DAPI) (Sigma) and cellular cytoskeleton (Alexa488-phallodin) were utilized to observe cell adhesion and spreading respectively. Primary anti-α-actin (G-12), anti-MYH11 (G-4), and anti-Calponin 1(CALP) antibodies were supplied through Santa Cruz Biotechnologies. Secondary antibodies conjugated with either Alexa 488 or Alexa 647 along with Alexa 488-phallodin cytoskeleton stain were acquired through Invitrogen, Inc. (Eugene, OR). Calponin and myosin heavy chain (MYH11) antigenic staining was performed to characterize SMC differentiation. For SMC marker immunostaining, samples were first incubated with primary anti-calponin or anti-MYH11 in 1% BSA overnight at 4° C. Following primary antibody coupling, samples were washed 3× in PBS and incubated with secondary antibody Alexa 488-IgG or Alexa 647-IgG for 2 h at room temperature. All samples were finally mounted with Fluoro-Gel (Electron Microscopy Services, Hatfield, PA) mounting medium and stored at 4°C for imaging.

2.4.3. Confocal imaging—Confocal images were acquired using a Nikon A1R laser scanning confocal microscope piloted by NIS-Elements 4.0 and equipped with 405 nm, 488 nm, 561 nm, and 640 nm laser lines. Unless otherwise stated, a 10× 0.5NA objective with the pinhole set to 1.2 Airy Units (AU) was used. When needed, multiple z planes were acquired in order to capture all of the cells within each SF hydrogel. A maximum intensity projection image or 3-dimensional rendering was then generated using ImageJ software.

2.5. Statistical analysis

All tests were performed in triplicate. Statistical significance of collected data was determined at each condition using an independent Student's t-test. Data are presented as mean ± standard deviation (SD) and was considered statistically significant at 95% confidence ($p < 0.05$). For qPCR, two-way ANOVA with Tukey's test was performed on

ΔCq values using Graphpad's Prism software. Error is represented by standard error of the mean for three replicates.

3. Results

In this study, the feasibility of using SF hydrogels with growth factor and tunable stiffness to promote vascular differentiation was evaluated. Silk hydrogels were prepared using high pressure CO_2, whereby gelation proceeds through the progressive reduction in solution pH achieved under CO_2-water binary systems [32]. We found that silk hydrogels prepared by this method require less time to gelation and display improved physical properties compared to conventional hydrogel fabrication methods. We note that while our technique allows for stable hydrogel formation at low silk protein water solution concentrations, our study revealed that silk concentrations less than 1.5 wt% resulted in nonhomogeneous gel formation (results not shown) and therefore were not practical for further evaluation. Consequently, hydrogels from silk concentrations 1.5, 2, 3 and 4 wt% (SF1.5, SF2, SF3, and SF4 respectively) were prepared for this study and assessed for physical and mechanical properties.

3.1. Hydrogel Fabrication and Characterization

The macrostructures of hydrogels prepared under high pressure CO_2 at various silk protein concentrations are shown in Figure 1. Visual observation of the silk hydrogels indicate stable gelation and mechanical integrity are retained for all protein concentrations investigated. Structural changes associated with silk hydrogel formation were confirmed by FTIR-ATR and displayed in Figure 2A. Evaluation of the spectral regions within 1700–1500 cm^{-1} relating to the peptide backbones of amide I (1700–1600 cm^{-1}) and amide II (1600–1500 cm^{-1}) are commonly utilized to observe the different secondary structures of SF [35]. The unprocessed silk solution displayed peaks centered at 1552 cm^{-1} (amide II) and 1654 cm^{-1} (amide I) indicating random coil and α-helix structures respectively. In contrast, silk hydrogels prepared by high pressure CO_2 resulted in peaks at 1625 cm^{-1} (amide I) and 1518 cm^{-1} (amide II) corresponding to silk II secondary structure and confirming the presence of extensive β-sheet crystals. Fourier self-deconvolution (FSD) analysis of the respective IR curves indicated a β-sheet content of 35± 2% for the SF1.5 hydrogel samples with a gradual increase to 46 ± 2% for the SF4 hydrogels. The increase in SF β-sheet content at greater protein concentrations has also been observed by others [39] and is likely due to increased protein macromolecular interactions resulting in enhanced β-sheet formation. Figure 2B displays the thermal scans obtained by DSC for both unprocessed SF solution (a) and silk hydrogels prepared by high pressure CO_2 (b–e). A broad endothermic peak between 60–90°C representing bound water was observed for all samples. Unprocessed SF solution revealed a non-isothermal crystallization peak at 225°C representing the transition of amorphous silk domains into β-sheet structures [35]. All silk hydrogel specimens lacked a glass transition region as well as crystallization peak due to the formation of extensive β-sheet structures during the CO_2 hydrogel fabrication process. Thermal degradation of the unprocessed silk solution occurred at a lower temperature (about 282 °C) compared to the gradual increase from 283°C to 289 °C for SF1.5 and SF4 hydrogels respectively. The lower degradation temperature observed for the SF1.5 samples compared to the SF4 specimens

agrees with the lower β-sheet content revealed by FTIR. Collectively, these observations indicate silk-CO_2 hydrogels exhibit extensive β-sheet crystal domains, permitting stable gel formation at all protein concentrations investigated.

3.2. Hydrogel Pore Characteristics

SF hydrogel morphology characteristics were evaluated using SEM in the dry state (Figure 3a–d) and compared against wet state imaging (Figure 3e–h) using CLSM. Dry state imaging revealed a porous matrix with average pore sizes ranging from 3.40 ± 0.58 - 4.97 ± 1.28 μm for all SF hydrogel concentrations. A slight decrease in pore size was observed for SF2 and SF3 hydrogel specimens at 3.40 ± 0.58 μm and 3.48 ± 0.42 μm average pore size, respectively. By comparison, the average pore sizes for SF1.5 and SF4 were greater at 4.97 ± 1.28 and 4.92 ± 0.83 μm, respectively. Analysis of SF hydrogel pore distributions were not found to be significantly different. Comparison of the dry state pore size and distribution were in good agreement with the complimentary measurements achieved using wet state imaging. The average pore sizes reported here correlate well with SF hydrogels prepared in our previous work [32].

3.3. Hydrogel Compressive Properties

To assess SF hydrogel mechanical properties, we evaluated the mechanical response of all specimens in compression. Figure 4a represents the stress-strain curves of SF1.5, SF2, SF3 and SF4 hydrogel specimens tested in compression. All SF hydrogel samples displayed a linear response up to 10% strain level, demonstrating the elasticity of fabricated hydrogels. The compressive modulus of the hydrogel samples increased as SF concentration increased (Figure 4b). The compressive modulus increased by 10-fold from SF1.5 (6.41 ± 0.47 kPa) to SF4 hydrogels (63.98 ± 2.42 kPa). The elastic moduli of SF hydrogels displayed here, ~6 – 64 kPa, represent a biologically relevant stiffness range for native vasculature, suggesting their potential use for vascular tissue engineering substrates [40].

3.4. Effect of SF Hydrogel Rigidity on hMSC attachment and spreading in Low-Serum or TGFβ-1 Fortified Media

Serum-containing media, including more defined serum mixtures for stem cell culture, is often not well defined, incorporating several combinations of factors as well as high variability among lots [41]. From this stance, serum-based differentiation protocols do not allow for unadulterated manipulation of the biochemical milieu necessary to define concise spatiotemporal microenvironments. Therefore, to suppress the potential for compounding effects of soluble factors, we chose low-serum (1% defined FBS) culture conditions for all experiments.

To confirm the biocompatibility of our SF hydrogels, we cultured hMSCs for 72 h in media either with low serum or TGF-β1 (+) (10ng/ml) supplemented low serum, and evaluated cell attachment and spreading (Figure 5a–h). Human MSC attachment was observed for all SF hydrogel formulations. Utilizing image analysis, we measured hMSC density after culturing on SF hydrogels for 72 h with variable stiffness. Human MSC density increased from 150 ± 30 cells/mm^2 to 622 ± 87 cells/mm^2 for 6 kPa (SF1.5) and 64 kPa (SF4) hydrogels in low-serum culture conditions respectively (Figure 5j). Likewise, supplementing low-serum

media with 10 ng/ml of TGF-β1 resulted in a significant ($p < 0.05$) increase in the cell density for all SF hydrogel elasticities studied with an increase from 427 ± 28 cells/mm^2 to 798 ± 26 cells/mm^2 for 6 kPa (SF1.5) and 64 kPa (SF4) hydrogels, respectively. This data suggests that hMSC attachment positively correlates with SF hydrogel stiffness and TGF-β1 administration.

Significant cell spreading was observed (Figure 5a–h) and distinct cellular morphologies revealed for all SF hydrogel samples (Figure 5i) irrespective of growth factor intervention. Cell spreading area was quantified using image analysis and normalized to the respective cell density of each specimen. We found no significant differences in cell spreading area for SF hydrogels of different stiffness or growth factor protocol with the exception of the 6 kPa (SF1.5) hydrogel under low-serum conditions. The discrepancy in cell spreading area for the 6 kPa (SF1.5) low-serum condition is likely due to the reduced cell density measured for these samples, which could facilitate enhanced cellular spreading throughout the substrate. Altogether, our findings suggest that the SF hydrogels produced here provide a sustainable microenvironment for hMSC attachment and spreading in the presence of low-serum or TGF-β1 fortified media.

3.5. Effect of SF Hydrogel Rigidity and TGF-β1 on Vascular SMC Commitment of hMSCs

Myogenic differentiation was evaluated by real time PCR and assessed for SMC-specific marker expression of smooth muscle α-actin (αSMA), calponin, and smooth muscle myosin heavy chain (MYH11) as shown in Figure 6a–c. Human MSCs cultured without TGF-β1 for 72 h on SF hydrogels displayed non-significant ($p > 0.05$) variation in αSMA and calponin gene expression for all elasticities investigated when compared to the culture plate control (Figure 6a–b). In contrast, in the absence of TGF-β1 administration the gene expression of the mature SMC marker, MYH11, was significantly ($p < 0.05$) upregulated on 33 kPa (SF3) substrate compared to the culture plate condition (Fig 6c).

Interestingly, the inclusion of 10 ng/ml of TGF-β1 did not result in significant variation of αSMA transcription levels for all SF hydrogels investigated, Figure 6a. However, a significant ($p < 0.05$) variation in calponin gene expression was recorded on 6 kPa soft hydrogel (SF1.5) with and without TGF-β1 as shown in Figure 6b. By comparison, the administration of TGF-β1 significantly ($p < 0.001$) upregulated MHY11 gene expression on 33 kPa (SF3) over all others, 6 kPa (SF1.5), 20 kPa (SF2), 64 kPa (SF4) and culture plate (Fig 6c). Further, a significant ($p < 0.05$) difference was also observed on 33 kPa (SF3) among TGF-β1 (+) and TGF-β1 (−) conditions. The greater variation of MHY11 gene expression for hMCSs cultured on SF hydrogels with TGF-β1 compared to TGF-β1 (−) conditions indicates that a crosstalk exists between physical cues (stiffness) and chemical stimuli (TGF-β1), which regulate hMSC fate decisions.

We further confirmed stem cell lineage commitment using the protein level expression of calponin and MHY11 for hMSCs cultured on SF hydrogels with TGF-β1 for 72 h (Figure 7). High levels of calponin were detected for SF1.5, SF2, SF3 hydrogels 6, 20, and 33 kPa stiffness respectively, Figure 7. Consistent with reported gene expression, MHY11 protein expression was detected for all SF hydrogel conditions with greatest expression on 33 kPa (SF3) substrate. Compared to softer SF hydrogels, calponin and MHY11 expression were

absent on stiff condition (SF4). Altogether, these results suggest that appropriate substrate stiffness and growth factor presentation can achieve mature and directed differentiation of hMSCs, specifically in the context of vascular SMCs.

4. Discussion

Stem cells develop an exquisite relationship with their surroundings which elicit an ensemble of cellular events influenced not only by the physical environment, such as rigidity [7] and geometry [10], but also the chemical makeup of their milieu through growth factors [13] and cytokines [5], amongst others [42]. Recent evidence suggests a complex interplay whereby matrix physical and chemical stimuli may work synergistically to direct highly specialized cellular events and fate outcomes [43, 14]. Therefore, resolving the effects associated with the crosstalk of physicochemical stimuli within the *in vivo* microenvironment may provide a template for the rational design of specialized and directed stem cell differentiation platforms. We chose to address these queries by examining the vascular fate commitment of hMSCs cultured on SF hydrogels of different stiffness in the presence of growth factor (TGF-β1) administration.

To minimize the compounding effects of other biological stimuli, we selected a substrate material that allowed for cellular attachment in the absence of defined biological ligands or serum proteins. The tunable properties of SF allow for the regulation of format and substrate mechanical properties with high fidelity, meanwhile highly biocompatible. In our hands, we find SF hydrogels prepared from a simple CO_2 processing technique to be a promising biomaterial platform for probing the effects of substrate stiffness and cell maintenance and fate commitment. Here we report tunable stiffness of our SF hydrogels by simple adjustment of the starting silk protein in water concentration. This observation is complimentary to previous studies using SF protein concentration to modulate substrate mechanical properties [21, 32]. When cultured with serum-starved media upon our SF hydrogels hMSCs attached and spread for up to 72 h (Supplementary Figure 1). This data suggests that SF is permissive to stem cell adhesion and maintenance irrespective to the presentation of adsorbed serum proteins or other biological ligands. The exact mechanism of hMSC adhesion and maintenance in low serum media demonstrated here on SF hydrogels is not readily apparent. Sengupta et al demonstrated an upregulation of integrin alpha-5 (ITGA5) in hMSCs cultured on SF patterned films [46], which may be a result of sparse RGY and RGV sequences previously identified in SF [47]. Recent reports have also demonstrated a potential CD44 interaction for fibroblasts [48] and rat MSCs [49] cultured on SF constructs. From the cited literature, it is likely that hMSC-SF interactions are a result of the unique material chemistry of SF. Future studies are needed to elucidate the distinct cellular interactions of specific cell lines, particularly stem cells, upon SF-based materials.

The TGF-β family regulates a diversity of cellular functions during development and tissue homeostasis through their effects on cell proliferation, differentiation, apoptosis and ECM production [34, 44]. Several reports have implicated TGF-β1 promoting MSC differentiation into SMC lineage [13, 45], and further evidence suggests that these TGF-β1 pathways may form a crosstalk with other signaling events elicited through mechanosensing stimuli such as substrate rigidity [43]. However, the role that these different micro-environmental factors

play independently and in concert towards mature vascular SMC differentiation has yet to be studied in a relevant platform for potential tissue engineering scaffolds such as SF hydrogel matrices.

In the absence of growth factor, we observed a positive correlation of cell density to SF substrate rigidity. This is consistent with other studies that have reported on elevated cell attachment and proliferation of hMSCs on substrates of variable stiffness [7]. Complimentary to these findings, the inclusion of 10 ng/ml of TGF-β1 to our cell culture regimen significantly ($p < 0.05$) increased cell density of hMSCs upon the SF hydrogels irrespective of stiffness. Interestingly, we did not find significant differences of hMSC spreading between groups (stiffness and TGF-beta) with the exception of the low stiffness condition (6 kPa). This observation may be attributed to the three-dimensional geometry conveyed by our SF hydrogels. Cell spreading and morphology in two dimensions are strongly correlated to stem cell differentiation and lineage commitment [7]; whereas, recent evidence suggests this phenomenon is less pronounced in three dimensions [10]. We note that while our porous SF hydrogels do not allow deep penetration of cells into the matrices, our system still mimics a three dimensional environment which may impart analogous geometrical cues as observed in other defined three dimensional substrates; thereby, resulting in similar cellular morphologies between groups.

Strikingly, we demonstrated a significant increase in both the gene and protein expression of the mature vascular SMC marker MHY11 for hMSCs cultured on SF hydrogel with 10 ng/ml TGF-β1 within 72 h. We observed a strong correlation of SF substrate stiffness to upregulate MHY11 expression both with and without TGF-β. For instance, MYH11 expression was detected on the gene level for soft (6 kPa, SF1.5) to mid-range stiff (33 kPa, SF3) SF hydrogels without growth factor regimens. However, the inclusion of TGF-β1 resulted in an approximate 12 fold increase in MHY11 gene expression for 33 kPa (SF3) hydrogel, whereas by comparison without TGF-β regimen only a 6 fold increase was detected. In contrast to the mature SMC phenotype marker MHY11, early SMC markers (αSMA) and (calponin) transcription levels were not significantly upregulated for all conditions, with the exception of 6 kPa (SF1.5) soft hydrogel, TGF-β1 (+) and TGF-β1 (−) groups. Consistent with our findings, Park et al. reported transcription levels for αSMA and calponin in hMSCs cultured with 10 ng/ml TGF-β on soft (15 kPa), two-dimensional gelatin substrates were comparable to transcription levels of the culture plate control [43].

As discussed earlier, we note that significant differences in cell density were reported for our SF hydrogel matrices. Cell-matrix and cell-cell interactions are widely believed to play important roles in various cellular processes, including differentiation. McBeath et al. revealed that hMSCs differentiated into either adipogenic or osteogenic lineages in the presence of conditioned media by adjusting initial cell seeding density; whereby, high cell densities led to adipogenesis and, by comparison, lower cell densities resulted in osteogenesis [50]. Along these lines, Xue et al. demonstrated that the promotion of osteogenic marker expression by rigid substrates could be overridden by a high seeding density [51]. Interestingly, cell density did not influence the chondrogenic marker expressions induced by soft substrates, indicating that lineage as well as specific matrix environments may be necessary to trigger cell-matrix and cell-cell crosstalk events. The

effects of cell density on the SMC commitment of hMSCs cultured on our SF matrices is not immediately understood. A systematic study evaluating cell density with SF matrix rigidity on the differentiation potential of hMSCs would help to elucidate the complex interplay of cell-matrix and cell-cell interactions.

Previously, authors have reported on directed hMSC differentiation towards myogenic lineage by regulating substrate stiffness [7] or combining with TGF-β1 administration [43]. However, these studies only investigated early (αSMA, calponin) myogenic markers, but often achieving directed stem cell differentiation towards a mature status is desired [52]. Stem cell differentiation into SMC-like populations is repeatedly evaluated by identifying the expression of several candidates involved in the contractile apparatus such as αSMA, h1-calponin, MYH11 and desmin [53]. However, recent evidence suggests that some SMC markers are potentially expressed at measurable levels in multipotent MSCs. For instance, MSCs cultured without differentiation media expressed mRNA levels for several SMC markers at levels comparable to primary SMCs, with the exception being the mature SMC marker MYH11 [54]. Indeed, MYH11 is only expressed late in myogenesis and displays the highest specificity of SMC differentiation compared to any other known marker [55]. Collectively, these recent findings suggest that mature markers such as MYH11 logically serve as a reliable indication of mature SMC phenotype in hMSCs as shown here.

Our results support the hypothesis that the convergence of physical and chemical environmental cues can lead to specific and directed differentiation of hMSCs into matured vascular SMCs. Our data suggests that proper substrate stiffness and growth factor (TGF-β) can significantly upregulate SMC genes and protein expression. We note that one limitation of our method is the potential differences of SF hydrogel water content or network density among the different hydrogel formulations. Recently, Wen et al. systematically modulated the porosity, ligand density and stiffness of polyacrylamide (PA) hydrogels and observed how these properties affect stem cell fate processes [56]. Here the author's concluded that stiffness rather than porosity or ligand density was the primary impetus driving stem cell differentiation. In line with this, while it is difficult to decouple certain physical parameters (i.e. porosity, network density) from our SF hydrogel formulations presented here, evidence suggests that substrate stiffness is the dominate physical parameter in directing stem cell fate, as demonstrated here.

Previous studies have highlighted a significant crosstalk between substrate rigidity and growth factor activity. Regulation of MSC commitment into chondrogenic or myogenic phenotypes on two dimensional matrices can be modulated based on substrate stiffness and TGF-β1 administration [43]. Recently, soft (2 kPa), three dimensional matrices combined with vascular endothelial growth factor (VEGF) were revealed to act synergistically to guide MSC differentiation into mature endothelial phenotype while enhancing paracrine signaling [14]. Indeed, there is growing evidence that a tight interplay exists between ECM mechanical properties and the activity and availability of several growth factors. It is well established that ECMs provide not only physical support for cellular processes but also act as a repository for a plethora of chemical signals [57]. For instance, TGF-β1 is believed to form a physical association with numerous ECM proteins and only through matrix straining, via cell contractile forces transmitted through integrins, is it liberated and active [58]. In line

with this, Wipff et al. demonstrated a positive correlation between TGF-β1 activation and polyacrylamide hydrogel stiffness for cultured fibroblast and epithelial cells [59]. Here the authors proposed a contraction-mediated activation of TGF-β1 whereby increasing ECM stiffness (i.e. polymer stiffness) resulted in increased levels of active TGF-β1. Nonetheless, it remains to be resolved how mechanical activation of TGF-β1 is achieved using our current SF hydrogel system. From the cited literature, there is evidence to suggest that ECM mechanics play a critical role in the deployment and activation of chemical signals in the cellular microenvironment. Our results are complimentary to these findings, whereby stem cell behavior can be regulated based on the integration of substrate physical and chemical properties.

Although others have reported on the differentiation of stem cells towards mature SMC lineage, our study advances these previous results in several ways. First, we explored the potential to direct specialized hMSC differentiation by modulating stiffness and growth factor using a well-defined biomaterial scaffold platform. In contrast to previous studies, our methodology employs SF, a well-tolerated biomaterial with an impressive portfolio of tissue engineering applications. Secondly, we demonstrate the expression of a mature SMC marker (MYH11) within the span of 72 h with appropriate substrate stiffness 33 kPa (SF3) and growth factor (10 ng/ml TGF-β1). By comparison, El-Mounayri et al. derived mature and functional human coronary-like vSMCs from embryonic stem cells (ESCs) using a complex growth factor regimen across 28 d [41]. We acknowledge the limitation that our study did not show the functional behavior of the SMC line derived here from hMSCs; however, our methodology suggests that complex differentiation protocols may be simplified by engineering the cellular microenvironment on multiple scales, i.e. matrix stiffness with growth factor. Third, it highlights the significance of designing multifaceted biomaterial matrices, culminating physical and chemical cues, to direct stem cell differentiation in a highly controlled and specialized approach.

5. Conclusion

There is a growing consensus that the next generation of biomaterial platforms must adopt a biomimetic approach whereby the integration of physical and chemical environmental cues becomes necessary to direct highly specialized cellular processes, including stem cell fate decisions. This study demonstrates the potential utility of SF hydrogels as a tunable platform, integrating physical (stiffness) and chemical (TGF-β1) stimuli, for directed and specialized differentiation of hMSCs. Our results demonstrate that SF hydrogels provide a permissive environment for hMSCs in the absence of serum media, meanwhile tunable in stiffness by simple adjustment of SF protein content. Further, we report on the ability to augment hMSC differentiation into mature SMCs within modest culture periods (72 h) by combining appropriate SF hydrogel stiffness (33 kPa) with growth factor (TGF-β1). This study advances our understanding of how complex multicomponent biomaterials, whereby mimicking the intricacy of natural tissue environments, can play a significant role in developing optimal stem cell differentiation protocols. Ultimately, such an understanding of how engineered cellular niche environments interact with stem cell fate processes will be instrumental in the design of future tissue engineering platforms.

Supplementary Material

Refer to Web version on PubMed Central for supplementary material.

Acknowledgments

The authors would like to acknowledge the financial support from the National Institute for Health K25HL097246 (W.T.) and R01 HL119371 (W.T.). The authors would also like to thank the BioFrontiers Advanced Light Microscopy Core for their excellent microscopy and imaging support.

References

1. Laslett LJ, Alagona P Jr, Clark BA 3rd, Drozda JP Jr, Saldivar F, Wilson SR, Poe C, Hart M. The worldwide environment of cardiovascular disease: prevalence, diagnosis, therapy, and policy issues: a report from the American College of Cardiology. J Am Coll Cardiol. 2012; 60:S1–S49. [PubMed: 23257320]
2. Bajpai VK, Andreadis ST. Stem Cell Sources for Vascular Tissue Engineering and Regeneration. Tissue Eng. Part B. 2012; 18:405–425.
3. O'Shea CA, Hynes SO, Shaw G, Coen BA, Hynes AC, McMahon J, Murphy M, Barry F, O'Brien T. Bolus delivery of mesenchymal stem cells to injured vasculature in the rabbit carotid artery produces a dysfunctional endothelium. Tissue Eng. Part A. 2010; 16:1657–1665. [PubMed: 20001215]
4. Breitbach M, Bostani T, Roell W, Xia Y, Dewald O, Nygren JM, Fries JW, Tiemann K, Bohlen H, Hescheler J, Welz A, Bloch W, Jacobsen SE, Fleischmann BK. Blood. 2007; 110:1362–1369. [PubMed: 17483296]
5. Discher DE, Mooney DJ, Zandstra PW. Growth factors, matrices, and forces combine and control stem cells. Science. 2009; 324:1673–1677. [PubMed: 19556500]
6. Kuraitis D, Giordano C, Ruel M, Musarò A, Suuronen EJ. Exploiting extracellular matrix-stem cell interactions: a review of natural materials for therapeutic muscle regeneration. Biomaterials. 2012; 33:428–443. [PubMed: 22014942]
7. Engler JA, Sen S, Sweeney HL, Discher DE. Matrix Elasticity Directs Stem Cell Lineage Specification. Cell. 2006; 126:677–689. [PubMed: 16923388]
8. Discher DE, Janmey P, Wang YL. Tissue cells feel and respond to the stiffness of their substrate. Science. 2005; 310:1139–1143. [PubMed: 16293750]
9. Cukierman E, Pankov R, Stevens DR, Yamada KM. Taking cell-matrix adhesions to the third dimension. Science. 2001; 294:1708–1712. [PubMed: 11721053]
10. Huebsch N, Arany PR, Mao AS, Shvartsman D, Ali OA, Bencherif SA, Rivera-Feliciano J, Mooney DJ. Harnessing traction-mediated manipulation of the cell/matrix interface to control stem-cell fate. Nat Mater. 2010; 9:518–526. [PubMed: 20418863]
11. Suzuki S, Narita Y, Yamawaki A, Murase Y, Satake M, Mutsuga M, Okamoto H, Kagami H, Ueda M, Ueda Y. Effects of extracellular matrix on differentiation of human bone marrow-derived mesenchymal stem cells into smooth muscle cell lineage: utility for cardiovascular tissue engineering. Cells Tissues Organs. 2010; 191:269–280. [PubMed: 19940434]
12. Gong Z, Niklason LE. Small-diameter human vessel wall engineered from bone marrow-derived mesenchymal stem cells (hMSCs). FASEB J. 2008; 22:1635–1648. [PubMed: 18199698]
13. Narita Y, Yamawaki A, Kagami H, Ueda M, Ueda Y. Effects of transforming growth factor-beta 1 and ascorbic acid on differentiation of human bone-marrow-derived mesenchymal stem cells into smooth muscle cell lineage. Cell Tissue Res. 2008; 333:449–459. [PubMed: 18607632]
14. Wingate K, Floren M, Tan Y, Tseng PON, Tan W. Synergism of Matrix Stiffness and Vascular Endothelial Growth Factor on Mesenchymal Stem Cells for Vascular Endothelial Regeneration. Tissue Eng Part A. 2014; 20:2503–2512. [PubMed: 24702044]
15. Philp D, Chen SS, Fitzgerald W, Orenstein J, Margolis L, Kleinman HK. Complex extracellular matrices promote tissue-specific stem cell differentiation. Stem Cells. 2005; 23:288–296. [PubMed: 15671151]

16. Kim TG, Shin H, Lim DW. Biomimetic scaffolds for tissue engineering. Adv. Funct. Mater. 2012; 22:2446–2468.
17. Place ES, Evans ND, Stevens MM. Complexity in biomaterials for tissue engineering. Nature Mater. 2009; 8:457–470. [PubMed: 19458646]
18. Laflamme MA, Murry CE. Heart regeneration. Nature. 2011; 473:326–335. [PubMed: 21593865]
19. Bouten CVC, Dankers PYW, Driessen-Mol A, Pedron S, Brizard AMA, Baaijens FPT. Substrates for cardiovascular tissue engineering. Adv. Drug. Deliver. Rev. 2011; 63:221–241.
20. Stegemann JP, Kaszuba SN, Rowe SL. Review: advances in vascular tissue engineering using protein-based biomaterials. Tissue Eng. 2007; 13:2601–2613. [PubMed: 17961004]
21. Kundu B, Rajkhowa R, Kundu SC, Wang X. Silk fibroin biomaterials for tissue regenerations. Adv. Drug. Deliv. Rev. 2013; 65:457–470. [PubMed: 23137786]
22. Meinel L, Fajardo R, Hofmann S, Langer R, Chen J, Snyder B, Vunjak-Novakovic G, Kaplan D. Silk implants for the healing of critical size bone defects. Bone. 2005; 37:688–698. [PubMed: 16140599]
23. Fini M, Motta A, Torricelli P, Giavaresi G, Nicoli Aldini N, Tschon M, Giardino R, Migliaresi C. The healing of confined critical size cancellous defects in the presence of silk fibroin hydrogel. Biomaterials. 2005; 26:3527–3536. [PubMed: 15621243]
24. Wang Y, Bella E, Lee CSD, Migliaresi C, Pelcaster L, Schwartz Z, Boyan BD, Motta A. The synergistic effects of 3-D porous silk fibroin matrix scaffold properties and hydrodynamic environment in cartilage tissue regeneration. Biomaterials. 2010; 31:4672–4681. [PubMed: 20303584]
25. Soffer L, Wang X, Zhang X, Kluge J, Dorfmann L, Kaplan DL, Leisk G. Silk-based electrospun tubular scaffolds for tissue-engineered vascular grafts. J. Biomater. Sci. Polym. Ed. 2008; 19:653–664. [PubMed: 18419943]
26. Bondar B, Fuchs S, Motta A, Migliaresi C, Kirkpatrick CJ. Functionality of endothelial cells on silk fibroin nets: Comparative study of micro- and nanometric fibre size. Biomaterials. 2008; 29:561–572. [PubMed: 17942151]
27. Bonani W, Maniglio D, Motta A, Tan W, Migliaresi C. Biohybrid nanofiber constructs with anisotropic biomechanical properties. J. Biomed. Mater. Res.: Part B Appl. Biomat. 2011; 96:276–286.
28. Unger RE, Wolf M, Peters K, Motta A, Migliaresi C, Kirkpatrick CJ. Growth of human cells on a non-woven silk fibroin net: a potential for use in tissue engineering. Biomaterials. 2004; 25:1069–1075. [PubMed: 14615172]
29. Yang Y, Chen X, Ding F, Zhang P, Liu J, Gu X. Biocompatibility evaluation of silk fibroin with peripheral nerve tissues and cells in vitro. Biomaterials. 2007; 28:1643–1652. [PubMed: 17188747]
30. Gotoh Y, Niimi S, Hayakawa T, Miyashita T. Preparation of lactose-silk fibroin conjugates and their application as a scaffold for hepatocyte attachment. Biomaterials. 2004; 25:1131–1140. [PubMed: 14615179]
31. Lawrence BD, Marchant JK, Pindrus MA, Omenetto FG, Kaplan DL. Silk film biomaterials for cornea tissue engineering. Biomaterials. 2009; 30:1299–1308. [PubMed: 19059642]
32. Floren ML, Spilimbergo S, Motta A, Migliaresi C. Carbon Dioxide Induced Silk Protein Gelation for Biomedical applications. Biomacromolecules. 2012; 13:2060–2072. [PubMed: 22657735]
33. Carmeliet P. Mechanisms of angiogenesis and arteriogenesis. Nature Med. 2000; 6:389–395. [PubMed: 10742145]
34. Derynck R, Feng X-H. TGF-β receptor signaling. Biochim Biophys Acta. 1997; 1333:105–150.
35. Hu X, Kaplan D, Cebe P. Determining Beta-Sheet Crystallinity in Fibrous Proteins by Thermal Analysis and Infrared Spectroscopy. Macromolecules. 2006; 39:6161–6170.
36. Elliott WH, Bonani W, Maniglio D, Motta A, Tan W, Migliaresi C. Silk Hydrogels of Tunable Structure and Viscoelastic Properties Using Different Chronological Orders of Genipin and Physical Cross-Linking. Applied Materials & Interfaces. 2015; 22:12099–12108. [PubMed: 25978549]
37. Chomczynski P, Sacchi N. Single-step method of RNA isolation by acid guanidinium thiocyanate-phenol-chloroform extraction. Anal. Biochem. 1987; 162:156–159. [PubMed: 2440339]

38. Livak KJ, Schmittgen TD. Analysis of relative gene expression data using real-time quantitative PCR and the 2(−Delta Delta C(T)) Method. Methods. 2001; 25:402–408. [PubMed: 11846609]
39. Matsumoto A, Chen J, Collette AL, Kim UJ, Altman GH, Cebe P, Kaplan D. Mechanisms of silk fibroin sol-gel transitions. J. Phys. Chem. B. 2006; 110:21630–21638. [PubMed: 17064118]
40. Wingate K, Bonani W, Tan Y, Bryant S, Tan W. Compressive elasticity of three dimensional nanofiber matrix directs mesenchymal stem cell differentiation to vascular cells with endothelial or smooth muscle cell markers. Acta Biomater. 2012; 8:1440–1449. [PubMed: 22266031]
41. El-Mounayri O, Mihic A, Shikatani EA, Gagliardi M, Steinbach SK, Dubois N, Dacosta R, Li RK, Keller G, Husain M. Serum-free differentiation of functional human coronary-like vascular smooth muscle cells from embryonic stem cells. Cardiovasc Res. 2013; 98:125–135. [PubMed: 23213107]
42. Phillips JE, Petrie TA, Creighton FP, Garcia AJ. Human mesenchymal stem cell differentiation on self-assembled monolayers presenting different surface chemistries. Acta Biomater. 2010; 6:12–20. [PubMed: 19632360]
43. Park JS, Chu JS, Tsou AD, Diop R, Tang Z, Wang A, Li S. The effect of matrix stiffness on the differentiation of mesenchymal stem cells in response to TGF-β. Biomaterials. 2011; 32:3921–3930. [PubMed: 21397942]
44. Roelen BA, Dijke P. Controlling mesenchymal stem cell differentiation by TGF family members. J Orthop Sci. 2003; 8:740–748. [PubMed: 14557946]
45. Kinner B, Zaleskas JM, Spector M. Regulation of smooth muscle actin expression and contraction in adult human mesenchymal stem cells. Exp Cell Res. 2002; 278:72–83. [PubMed: 12126959]
46. Sengupta S, Park SH, Seok GE, Patel A, Numata K, Lu CL, Kaplan D. Quantifying osteogenic cell degradation of silk biomaterials. Biomacromolecules. 2010; 11:3592–3599. [PubMed: 21105641]
47. Zhou C, Confalonieri F, Jacquet M, Perasso R, Li Z, Janin J. Silk fibroin: Structural implications of a remarkable amino acid sequence. Proteins. 2001; 44:119–122. [PubMed: 11391774]
48. Yang MC, Chi NH, Chou NK, Huang YY, Chung TW, Chang YL, Liu HC, Shieh MJ, Wang SS. The influence of rat mesenchymal stem cell CD44 surface markers on cell growth, fibronectin expression, and cardiomyogenic differentiation on silk fibroin - Hyaluronic acid cardiac patches. Biomaterials. 2010; 31:854–862. [PubMed: 19857893]
49. Yang H, Yuan SS, Chung TW, Jong SB, Lu CY, Tsai WC, Chen WC, Lin PC, Chiang PW, Tyan YC. Characterization of silk fibroin modified surface: A proteomic view of cellular response proteins induced by biomaterials. BioMed. Res. Int. 2014; 2014:209469. [PubMed: 24818131]
50. McBeath R, Pirone DM, Nelson CM, Bhadriraju K, Chen CS. Cell shape, cytoskeletal tension, and RhoA regulate stem cell lineage commitment. Dev Cell. 2004; 6:483–495. [PubMed: 15068789]
51. Xue R, Li JY, Yeh Y, Yang L, Chien S. Effects of matrix elasticity and cell density on human mesenchymal stem cells differentiation. J. Orthop. Res. 2013; 31:1360–1365. [PubMed: 23606500]
52. Andreadis ST. Give your heart a chance: match the muscle to the vessel. Cardiovascular Research. 2013; 98:1–2. [PubMed: 23425515]
53. Liu Y, Deng B, Zhao Y, Xie S, Nie R. Differentiated markers in undifferentiated cells: Expression of smooth muscle contractile proteins in multipotent bone marrow mesenchymal stem cells. Dev Growth Differ. 2013; 55:591–605. [PubMed: 23557080]
54. Tamama K, Sen CK, Wells A. Differentiation of bone marrow mesenchymal stem cells into the smooth muscle lineage by blocking ERK/MAPK signaling pathway. Stem Cells Dev. 2008; 17:897–908. [PubMed: 18564029]
55. Owens GK, Kumar MS, Wamhoff BR. Molecular regulation of vascular smooth muscle cell differentiation in development and disease. Physiol. Rev. 2004; 84:767–801. [PubMed: 15269336]
56. Wen JH, Vincent LG, Fuhrmann A, Choi YS, Hribar KC, Taylor-Weiner H, Chen S, Engler AJ. Interplay of matrix stiffness and protein tethering in stem cell differentiation. Nat. Mater. 2014; 13:979–987. [PubMed: 25108614]
57. Martino MM, Briquez PS, Guc E, Tortelli F, Kilarski WW, Metzger S, Rice JJ, Kuhn GA, Müller R, Swartz MA, Hubbell JA. Growth factors engineered for super-affinity to the extracellular matrix enhance tissue healing. Science. 2014; 343(2014):885–888. [PubMed: 24558160]

58. Hinz B. The matrix and the transforming growth factor: tale of a strained relationship. Matrix Biol. 2015 [e-pub ahead of print].

59. Wipff PJ, Rifkin DB, Meister JJ, Hinz B. Myofibroblast contraction activates latent TGF-beta1 from the extracellular matrix. J. Cell Biol. 2007; 179:1311–1323. [PubMed: 18086923]

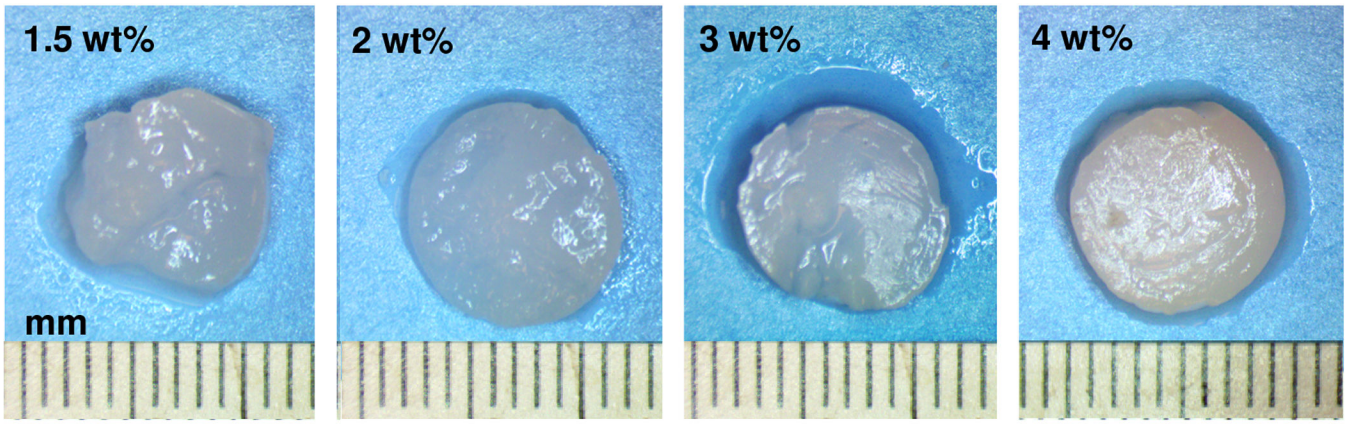

Figure 1. Gel images

Gross characterization of SF hydrogel matrices prepared at different protein concentrations.

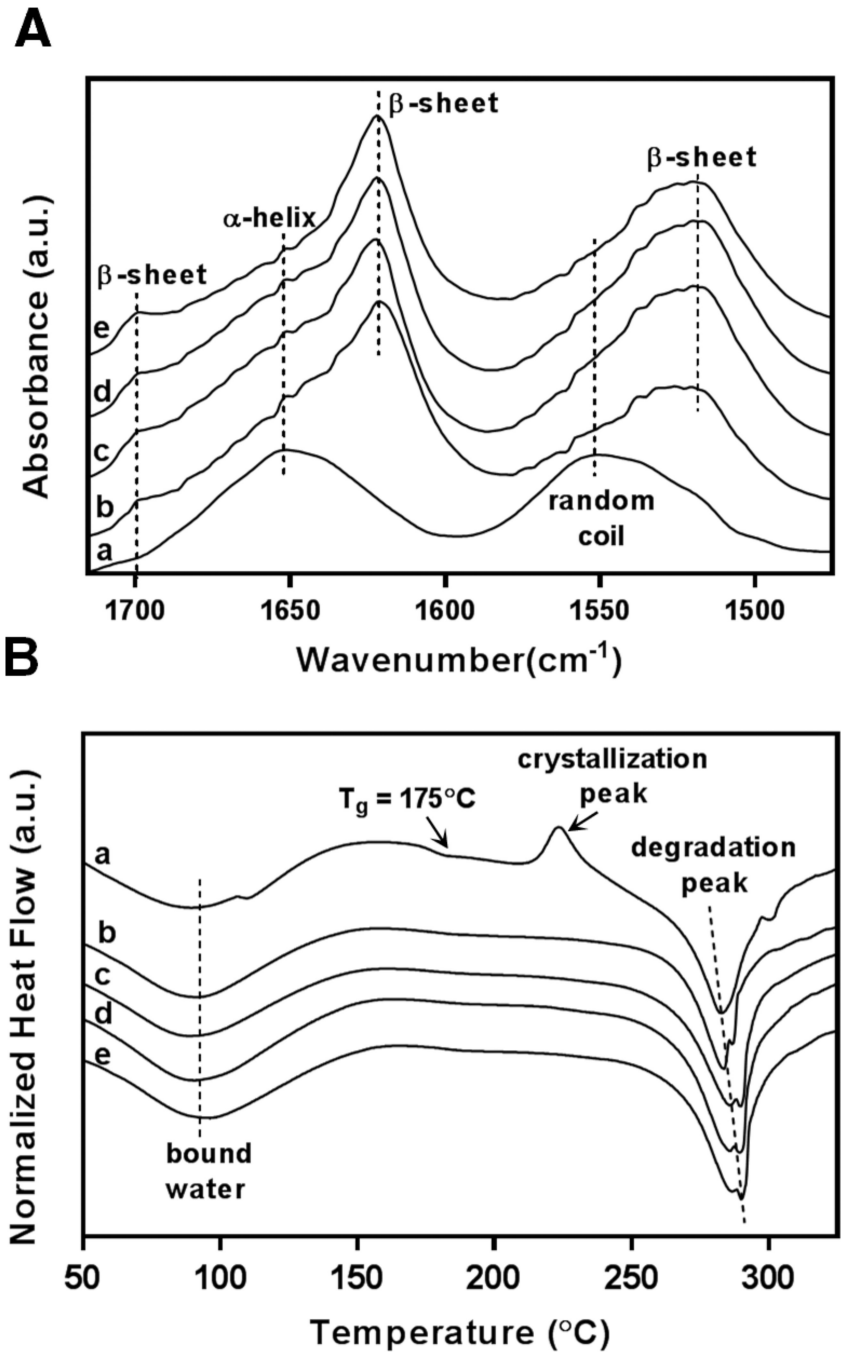

Figure 2. FTIR. DSC

Structural properties of SF hydrogels prepared by high pressure CO_2. (A) FTIR-ATR spectra reveal the presence of extensive β-sheet crystalline secondary structures in prepared hydrogel specimens; unmodified silk solution (a), prepared silk hydrogels SF1.5 (b), SF2 (c), SF3 (d), and SF4 (e). (B) DSC curves demonstrate stability under thermal scans for unmodified silk solution (a) and prepared silk hydrogels SF1.5 (b), SF2 (c), SF3 (d), and SF4 (e).

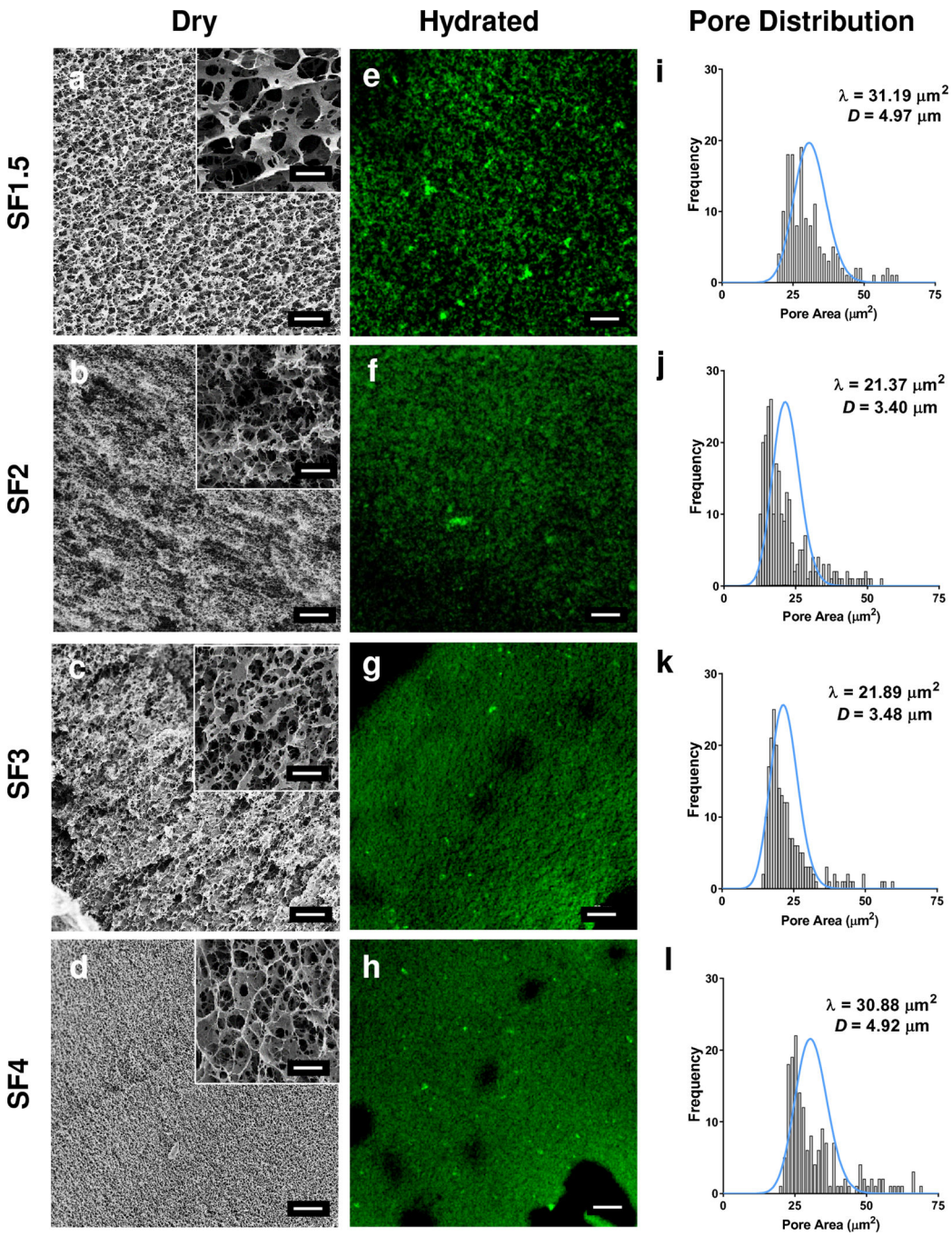

Figure 3. Hydrogel Morphology Assessment

Morphology assessment of silk hydrogel matrices. (a–d) Scanning electron microscopy images of silk hydrogels in dry state; inset magnification scale bars 5 μm. (e–h) Hydrated silk hydrogel images obtained by confocal laser microscopy. Scale bars 20 μm. (i–l) Silk hydrogel pore distributions, with respective Poisson distributions (blue lines), and pore size quantified by image analysis of respective micrographs (a–h).

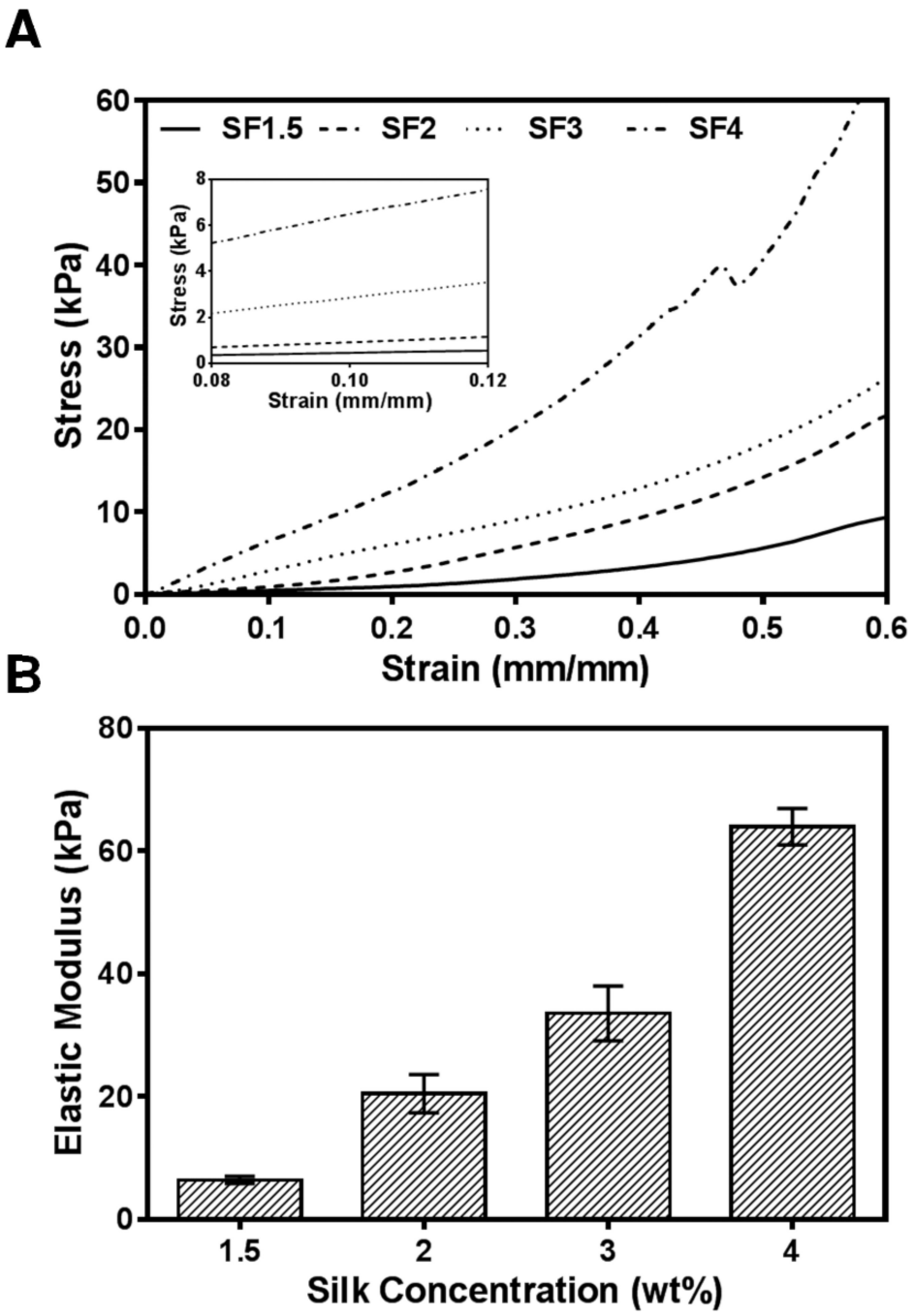

Figure 4. Hydrogel Compressive Data

Mechanical properties of SF hydrogels prepared by high pressure CO_2. (A) Stress vs. strain relationships for several hydrogel matrices prepared with different silk protein content. Inset represents linear region used to determine mechanical properties. (B) Elastic moduli of these matrices.

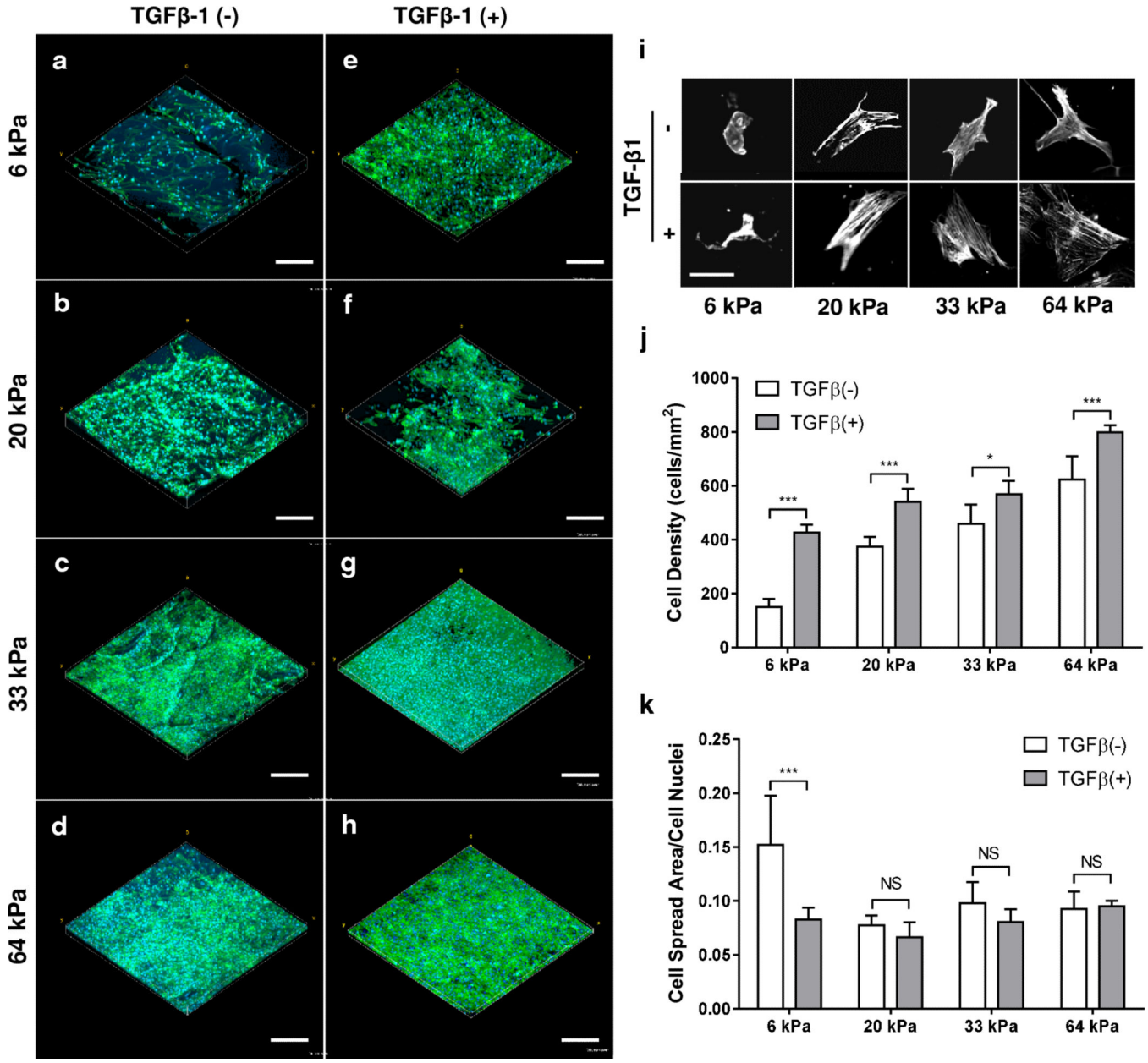

Figure 5. Cell Morphology Assessment

Effects of SF hydrogel stiffness and TGF-β1 on attachment and spreading of hMSCs. (a–h) Confocal stack renderings of hMSCs with (e–h) or without (a–d) TGF-β1 at various SF hydrogel elasticities (SF1.5-6kPa, SF2-20kPa, SF3-33kPa, SF4-64kPa). Cells were stained for cell nuclei (DAPI, blue) and F-actin (phalloidin, green), scale bar 300 μm. (i) Initial hMSC morphologies after 24 h seeding imaged and presented in grayscale with respect to SF hydrogel stiffness and TGF-β1 administration; scale bar 50 μm. Cell density (j) and attachment (k) of hMSCs for all the hydrogel matrices shown in images a–h were quantified and tabulated. * $P < 0.05$, *** $P < 0.001$, NS $P > 0.05$.

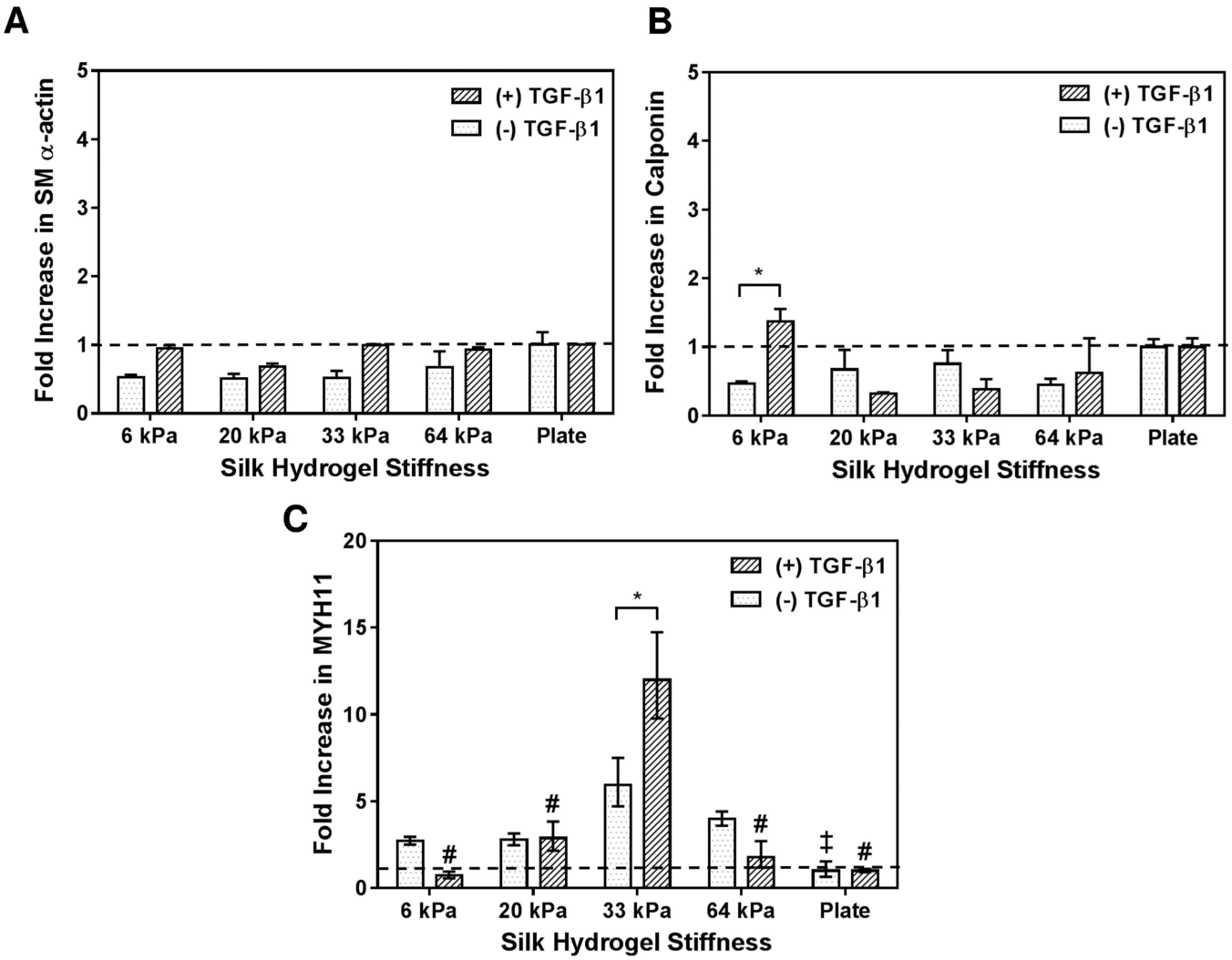

Figure 6. PCR data

PCR assessment of selected vascular markers of hMSCs cultured on silk hydrogels of different stiffness for 72 h: (a) smooth muscle α-actin, (B) calponin, and (C) MYH11. * indicates significant difference between groups ($p < 0.05$). ‡ indicates significant ($p < 0.05$) difference from the gene expression for hMSCs cultured without TGF-β1 on SF hydrogels compared to 33 kPa (SF3) condition. # indicates significant ($p < 0.001$) difference in gene expression for hMSCs cultured with TGF-β1 on SF hydrogels compared to 33 kPa (SF3) condition.

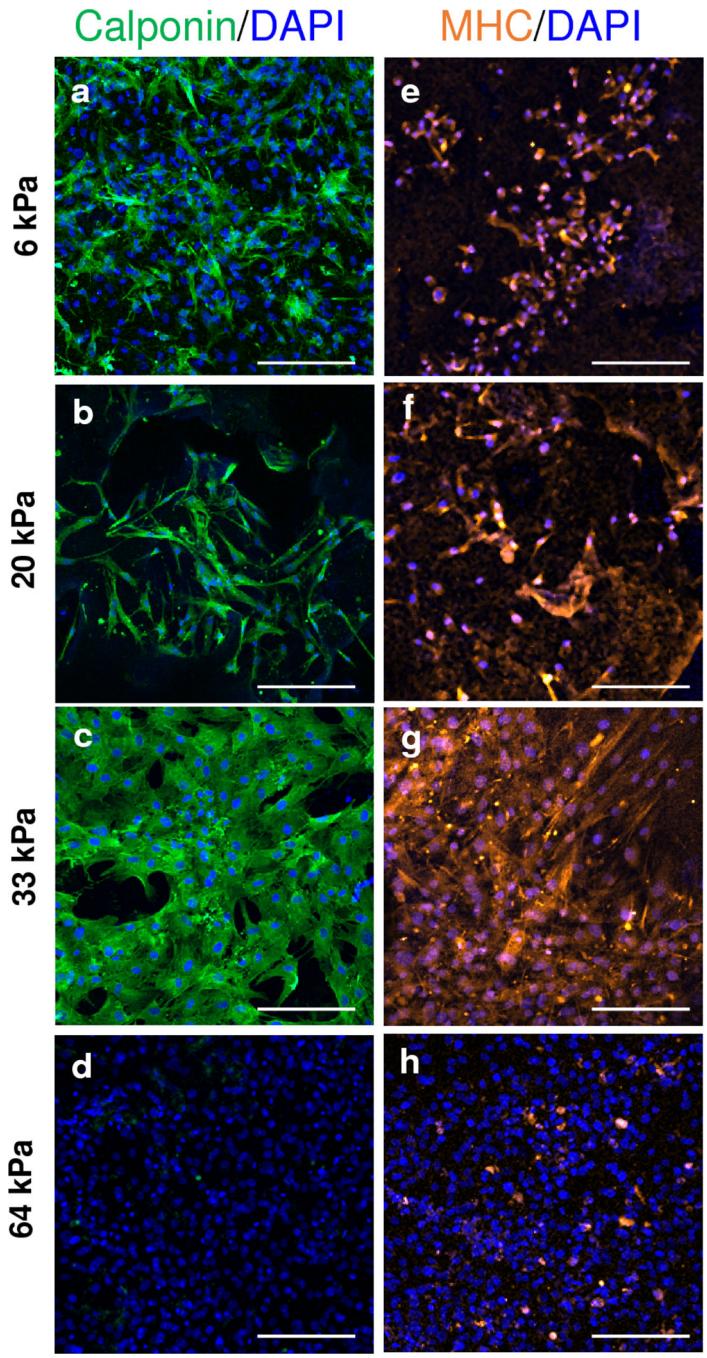

Figure 7. Immunostaining of select vascular markers

Immunostaining of hMSCs cultured with TGF-β1 on SF hydrogels of different stiffness for 72 h for select vascular SMC markers: calponin (a–d) (green), MYH11 (e–h) (orange). Scale bar 200 μm.

Table 1

Gene information for qPCR

Gene	Symbol	Ref Seq no.
Actin, beta	*ACTB*	NM_001101.3
Actin, alpha 2, smooth muscle, aorta	*ACTA2*	NM_001613.2
Calponin 1, basic, smooth muscle	*CNN1*	NM_001299.4
Myosin, heavy chain 11, smooth muscle	*MYH11*	NM_022844.2